Lyapunov spectrum of the driven Lorentz gas

Ch. Dellago,* L. Glatz,† and H. A. Posch‡
Institut für Experimentalphysik, Universität Wien, Boltzmanngasse 5, A-1090 Wien, Austria
(Received 20 April 1995)

A method for the evaluation of the full Lyapunov spectrum of an externally driven system with a hard-core interaction is presented. It is applied to the periodic Lorentz gas subjected to a homogeneous field and coupled to a Gaussian thermostat. The algorithm treats both the intercollisional streaming and the hard-core collisions exactly and can be easily generalized to many-body systems in nonequilibrium steady states interacting with hard-core potentials. From the Lyapunov spectrum of the Lorentz gas, the information dimension and the associated dimensionality reduction of the underlying fractal attractor were determined and compared to independent box-counting estimates for the same quantities.

PACS number(s): 05.45.+b, 02.70.Ns, 05.20.−y

I. INTRODUCTION

The Lorentz gas is one of the simplest models for transport phenomena in deterministic systems and has attracted considerable attention as a paradigm in the past decade [1–4]. It consists of a point particle moving in an array of hard scatterers on which it is elastically reflected and is a model for a noninteracting electron gas moving through a crystal. The transport properties of this model have been studied both in equilibrium in terms of Green-Kubo integrals and in nonequilibrium steady states. In the latter case nonequilibrium molecular dynamics methods have been applied: The system is externally perturbed, thus generating nonequilibrium fluxes from which transport coefficients such as the electrical conductivity [5–7] and the shear viscosity [8–10] can be determined. Due to the absence of a dissipating mechanism, the moving particle extracts energy from the field and its kinetic energy grows without bound. To prevent this divergence and to enforce a steady state, a heat bath is coupled to the system. This may be accomplished in different ways [11,12]. In this paper we follow the Lorentz-gas tradition and add a Gaussian thermostat to the equations of motion.

It has been shown that the phase space probability distribution of a thermostatted nonequilibrium system with time-reversible equations of motion has multifractal properties, which can be characterized by the set of Rényi dimensions or, equivalently, by the spectrum of singularities [13,14]. In equilibrium, where the model has very strong hyperbolic properties [15,16], as well as in most nonequilibrium steady states, the system turns out to be chaotic with a positive maximum Lyapunov exponent. This exponent describes the mean divergence rate of neighboring trajectories in phase space and is a measure for the sensitivity of the system trajectory to small perturbations of the initial conditions. There is an intimate relationship between the transport properties of a system and its Lyapunov spectrum both in equilibrium [4,17,18] and in nonequilibrium steady states [5,13]. Furthermore, the conjecture of Kaplan and Yorke permits the determination of the information dimension D_1 of the underlying attractor in phase space from the Lyapunov spectrum. Especially for high-dimensional systems, for which the estimation of fractal dimensions with box-counting methods becomes prohibitively expensive, this represents the only practical way for the estimation of attractor dimensions.

For the calculation of Lyapunov spectra of differentiable dynamical systems, the algorithm proposed by Benettin *et al.* [19,20] has become a well established and classic method. However, it has been noted by various authors [5,7] that the direct application of this method to systems with singular potentials such as for the Lorentz gas poses severe problems. Until recently the full Lyapunov spectrum of the Lorentz gas has only been determined with approximate and not very powerful methods. (a) In the equilibrium case the maximum Lyapunov exponent can be calculated by a method proposed by Sinai, which is based on following the temporal evolution of the curvature of a "wave front" propagating through the system [18]. Although suitable for equilibrium systems, this method is not easily applicable to nonequilibrium states and furthermore has the disadvantage of yielding only the maximum exponent. (b) Another attempt to overcome the problem caused by the singular potential has been the replacement with a very steep but smooth potential [7]. Also this approach requires considerable computational effort and furthermore requires an extrapolation. (c) It is also possible to estimate the Lyapunov spectrum of the nonequilibrium Lorentz gas by taking the detour over the calculation of the information dimension by means of a box-counting algorithm. The Kaplan-Yorke conjecture for D_1 and the relation of the

*Electronic address: dellago@ls.exp.univie.ac.at
†Present address: Institut für Mechanik, Technische Universität Wien, Wiedner Hauptstraße 8-10/325, A-1040 Wien, Austria. Electronic address: lglatz@mch2ws2.tuwien.ac.at
‡Electronic address: posch@ls.exp.univie.ac.at

spectrum with the relevant transport coefficient provide two independent equations for the determination of the two nonvanishing exponents (see below). However, this method is not very accurate and is computationally expensive. (d) Various authors have estimated Lyapunov exponents with an expansion of the dynamics in terms of unstable periodic orbits [21,22]. (e) Very recently Lloyd *et al.* [23] extended this method and suggested an exact scheme for the evaluation of the Lyapunov spectrum of the nonequilibrium Lorentz gas. It is based on the construction of a two-dimensional Poincaré map of sections for the phase flow defined by the collisions of the moving point particle with the scatterers and the subsequent stability analysis of this analytically derived transformation mapping one collision onto the next.

In this paper we present a method for the evaluation of the full Lyapunov spectrum of a nonequilibrium system interacting with elastic hard-core potentials. It treats both the streaming of the trajectory and the hard-core collisions exactly and for the externally driven Lorentz gas is equivalent to method (e) mentioned above. However, it does not require the analytical construction of a Poincaré map but treats the flow in the whole phase space. Only the equations of motion are needed as input. The method is a simple generalization of an algorithm devised for equilibrium systems by two of the present authors [24]. Due to its simplicity, our method may be easily adapted to the study of other transport phenomena in externally driven systems with hard-core interactions and/or many-body systems involving a high-dimensional phase space [25].

In Sec. II the driven Lorentz gas is defined. It serves as a test case for our algorithm and for our general approach to the problem of calculating Lyapunov spectra for nonequilibrium hard-core systems in an exact manner. Section III provides the necessary definitions and relations of the Lyapunov spectrum with other observables. The algorithm is derived in Sec. IV and the results for the Lorentz gas are presented and discussed in Sec. V. Section VI provides a short summary.

II. EXTERNALLY DRIVEN LORENTZ GAS

We consider a point particle with mass m, which moves with constant velocity v on a plane covered with a regular arrangement of hard disks with radius R. Their centers are located on the sites of a triangular lattice with lattice constant a. When the particle, referred to as the wanderer, collides with a scatterer it is elastically reflected. For a given disk radius R the geometry of the system is defined in terms of the density $\rho = 1/A$, where $A = \sqrt{3}a^2/2$ is the area of the hexagonal elementary cell of the lattice. The geometry is shown in Fig. 1

The wanderer is subjected to a spatially homogeneous and temporally constant field $\mathbf{E}$ acting on a positive unit charge. Since the particle extracts energy from the field, its kinetic energy increases proportionally to the distance from the starting point in field direction. To prevent this growth, a heat bath in the form of a Gaussian thermostat is coupled to the system. This leads to the equations of motion [5]

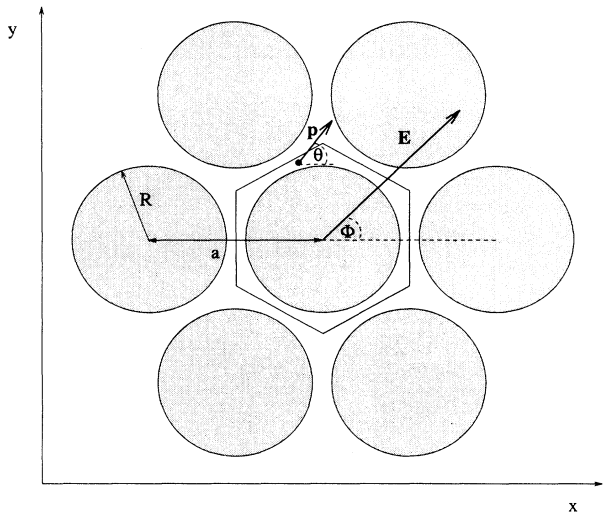

FIG. 1. The geometry of the periodic Lorentz gas.

$$\begin{aligned} \dot{x} &= p_x/m, \\ \dot{y} &= p_y/m, \\ \dot{p}_x &= E_x - \zeta p_x, \\ \dot{p}_y &= E_y - \zeta p_y, \\ \zeta &= \mathbf{E}\cdot\mathbf{p}/\mathbf{p}^2. \end{aligned} \tag{1}$$

The thermostat terms on the right-hand side of the momentum equations contain the fluctuating thermostat variable ζ and dissipate the extra energy gained from the field $\langle\zeta\rangle > 0$. Equations (1) conserve the kinetic energy. In polar coordinates

$$\begin{aligned} p &= \sqrt{p_x^2 + p_y^2}, \\ \theta &= \arctan\left(\frac{p_y}{p_x}\right), \end{aligned} \tag{2}$$

the equations of motion become

$$\begin{aligned} \dot{x} &= (p/m)\cos\theta, \\ \dot{y} &= (p/m)\sin\theta, \\ \dot{\theta} &= \left(E_y\cos\theta - E_x\sin\theta\right)/p, \\ \dot{p} &= 0. \end{aligned} \tag{3}$$

They can be solved analytically

$$\begin{aligned} x(t) &= x_0 - \frac{p^2}{mE}\left[\cos(\phi)\ln\left(\frac{\sin(\theta-\phi)}{\sin(\theta_0-\phi)}\right) - \sin(\phi)\,(\theta-\theta_0)\right], \\ y(t) &= y_0 - \frac{p^2}{mE}\left[\sin(\phi)\ln\left(\frac{\sin(\theta-\phi)}{\sin(\theta_0-\phi)}\right) + \cos\phi\,(\theta-\theta_0)\right], \\ \theta(t) &= 2\arctan\left\{\tan\left(\frac{\theta_0-\phi}{2}\right)\exp\left[-\frac{E}{p}\,(t-t_0)\right]\right\} + \phi, \\ p(t) &= p_0, \end{aligned} \tag{4}$$

where ϕ is the angle between the field direction and the positive x axis. The lower index 0 refers to the respective quantity at initial time t_0.

The trajectory of the wanderer is smooth between the collisions but changes noncontinuously during the collisions with the scatterer. This necessity of switching repeatedly from a soft to a hard potential and back complicates the problem. For the field-free case the location of the collision point and the determination of the collision parameters can be reduced to the solution of a quadratic equation. In the presence of an external field and a thermostat, the intercollisional segments of the trajectory are not straight lines any longer and more refined methods have to be applied in the simulation. We will return to this point in the next section.

This sequence of smooth streaming segments and discrete collisions must be taken into account also for the calculation of the Lyapunov spectrum. For this purpose we generalize the classic method of Benettin *et al.* [19,20].

III. LYAPUNOV EXPONENTS

In a chaotic system two nearby phase space trajectories separate on the average exponentially with time. For a differentiable N-dimensional dynamical system defined by

$$\dot{\mathbf{\Gamma}}(t) = \mathbf{F}(\mathbf{\Gamma}(t)), \tag{5}$$

the temporal evolution of a tangent vector $\boldsymbol{\delta}(t)$ connecting two differentially separated trajectories of the system is the solution of the linearized equations of motion

$$\dot{\boldsymbol{\delta}}(t) = \left.\frac{\partial \mathbf{F}}{\partial \mathbf{\Gamma}}\right|_{\mathbf{\Gamma}=\mathbf{\Gamma}(t)} \boldsymbol{\delta}(t). \tag{6}$$

$\mathbf{\Gamma}(t)$ is the *reference* trajectory in phase space, $\boldsymbol{\delta}(t)$ will be referred to as an *offset vector*, and $\mathbf{D} = \partial \mathbf{F}/\partial \mathbf{\Gamma}$ is the $N \times N$ Jacobi matrix of the system. In the following a trajectory displaced from the reference trajectory $\mathbf{\Gamma}(t)$ by an offset vector $\boldsymbol{\delta}(t)$ is referred to as a *satellite* trajectory.

The matrix $\mathbf{D}$ depends on the instantaneous state vector $\mathbf{\Gamma}(t)$. As demonstrated by Oseledec [26], there exists a set of N initial offset vectors $\boldsymbol{\delta}_l(0)$, $l = 1, \ldots, N$, such that the numbers

$$\lambda_l = \lim_{t\to\infty} \frac{1}{t} \ln \frac{|\boldsymbol{\delta}_l(t)|}{|\boldsymbol{\delta}_l(0)|} \tag{7}$$

exist. Furthermore, these so-called Lyapunov exponents are independent of the metric, the coordinate system, and the initial conditions. Usually they are ordered $\lambda_1 \geq \lambda_2 \geq \cdots \geq \lambda_N$ and the whole set is referred to as the Lyapunov spectrum.

Lyapunov spectra for symplectic systems (such as Hamiltonian systems in thermal equilibrium) exhibit a pronounced symmetry [27] $\lambda_l = -\lambda_{N+1-l}$, which we refer to as Smale pairing [28] (to acknowledge the contributions of Smale in clarifying the role of expanding and contracting motions in tangent space characteristic of chaotic time-reversible dynamical systems) and is also known as conjugate pairing [29]. In this case only the positive branch of the spectrum needs to be calculated. This symmetry is modified for externally driven and thermostatted homogeneous systems [29] and is totally lost for inhomogeneous systems [30]. Some of the Lyapunov exponents vanish. In every autonomous dynamical system there is at least one vanishing Lyapunov exponent, which corresponds to nonexponential expansion and contraction properties in the direction of the flow. Furthermore, possible constants of the motion cause additional exponents to vanish. This is treated in detail in Ref. [25].

The phase space for the Lorentz gas is four dimensional $\mathbf{\Gamma}(t) = \{x, y, p_x, p_y\}$ and there are four Lyapunov exponents. One of the exponents vanishes because of the nonexponential behavior in the flow direction as mentioned above. A second exponent vanishes as a consequence of the conserved kinetic energy (or the momentum norm) of the wanderer particle and the full spectrum can be reduced to $\{\lambda_{\max}, 0, 0, \lambda_{\min}\}$. In the field-free case ($E = 0$) one has $\lambda_{\max} = -\lambda_{\min}$, whereas for the driven system $\lambda_{\max} + \lambda_{\min} < 0$.

One of the most interesting aspects of the Lyapunov spectrum concerns its relation to the transport properties of the system [27]. The conductivity κ for the driven Lorentz gas is defined by

$$\kappa = \frac{\mathbf{E} \cdot \langle \mathbf{p} \rangle}{m |\mathbf{E}|^2}, \tag{8}$$

where $\langle\,\rangle$ denotes a time average. Since the sum of the Lyapunov exponents is equal to the phase space divergence of the original phase flow [11,12]

$$\sum_{l=1}^{N} \lambda_l = \left\langle \boldsymbol{\nabla}_{\mathbf{\Gamma}} \cdot \dot{\mathbf{\Gamma}} \right\rangle = -\frac{\mathbf{E} \cdot \langle \mathbf{p} \rangle}{p^2}, \tag{9}$$

one finds for the Lorentz gas

$$\kappa = -\frac{p^2}{m |\mathbf{E}|^2} (\lambda_{\max} + \lambda_{\min}) > 0. \tag{10}$$

Another quantity intimately related to the Lyapunov spectrum is the *information dimension* D_1 of the underlying strange attractor typical for nonequilibrium steady states of dissipative systems. In the case of the driven Lorentz gas it was found that the Hausdorff dimension D_0 is equal to the dimension of the embedding phase space [14], but that the information dimension D_1 is considerably smaller. Kaplan and Yorke conjectured that the dimension D_{KY} derived from the Lyapunov spectrum

$$D_{\mathrm{KY}} = n + \frac{\sum_{l=1}^{n} \lambda_l}{|\lambda_{n+1}|}, \tag{11}$$

with n the largest integer for which $\sum_{l=1}^{n} \lambda_l \geq 0$, provides a good estimate for the information dimension D_1. In our four-dimensional phase space with two vanishing exponents this gives

$$D_1 \approx D_{\mathrm{KY}} = 3 + \frac{\lambda_{\max}}{|\lambda_{\min}|}. \tag{12}$$

The information dimension D_1 is only one of an infinite

set of Rényi dimensions D_q [31,32]

$$D_q = \frac{1}{1-q} \lim_{\epsilon \to 0} \frac{\ln \sum_i p_i^q}{\ln \epsilon}, \tag{13}$$

where ϵ is the sidelength of hypercubes covering the entire attractor and p_i is the probability of finding the attractor in the ith box. Equivalently, the multifractal nature of the attractor can be characterized by the so-called singularity spectrum $f(a)$. Loosely speaking, this quantity is the fractal dimension of the set of points for which the probability distribution diverges with singularity strength a, i.e., $p_i \propto \epsilon^{-a}$ [33]. Chabra and Jensen have devised a method for the calculation of D_q and $f(a)$ [34]. In this paper we apply this method and compute D_1 from the singularity spectrum in order to compare it with D_{KY} obtained from the Lyapunov spectrum via the Kaplan-Yorke conjecture.

IV. ALGORITHM

We now turn to the practical calculation of the Lyapunov spectrum. Starting from definition (7) with an arbitrary vector $\boldsymbol{\delta}_l(0)$ one obtains the largest Lyapunov exponent λ_1 of the system. Similarly, the growth rate of a two-dimensional area element spanned by two arbitrary offset vectors is given by $\lambda_1 + \lambda_2$ and the sum $\sum_{l=1}^{k} \lambda_l$ is the growth rate of a k-dimensional volume element. For the calculation of the full spectrum it is necessary to follow the temporal evolution of a complete set of linearly independent offset vectors $\{\boldsymbol{\delta}_l\}$. Due to the continuous stretching and folding, initially orthonormal vectors tend to align in the direction of the vector corresponding to the maximum exponent and, furthermore, diverge exponentially. This can be avoided by a periodic reorthonormalization of the offset vectors. The Lyapunov exponents are obtained from the time average of the normalization factors for the offset vectors [19,20].

To apply this algorithm to our system, the temporal evolution of the offset vectors must be determined for both the smooth intercollisional streaming segments and the discrete elastic collisions with the scatterers. Between the collisions the equations of motion for the offset vectors are obtained by differentiating Eq. (1) with respect to the independent variables

$$\dot{\boldsymbol{\delta}} \equiv \begin{pmatrix} \delta\dot{x} = \delta p_x/m \\ \delta\dot{y} = \delta p_y/m \\ \delta\dot{p}_x = \frac{1}{p^4}\left[E_y\left(p_y^2 - p_x^2\right) + 2E_x p_x p_y\right](p_x\delta p_y - p_y\delta p_x) \\ \delta\dot{p}_y = \frac{1}{p^4}\left[E_x\left(p_x^2 - p_y^2\right) + 2E_y p_y p_x\right](p_y\delta p_x - p_x\delta p_y) \end{pmatrix}. \tag{14}$$

For simplicity we use in this paper a standard ordinary differential equation integrator for the integration of the reference trajectory and of the four offset vectors *between successive collisions.* Of course, a collision-by-collision approach would also be possible, but is more tedious to program [5].

A totally different approach has to be used for the effect the collisions exert on the offset vectors $\boldsymbol{\delta}$. First we note that the reference trajectory undergoes the noncontinuous change

$$\mathbf{q} \to \mathbf{q}, \quad \mathbf{p} \to \mathbf{p}'. \tag{15}$$

Here and in the following expressions the prime denotes a vector obtained by specular reflection on the surface of the scatterer. In order to find the transformation rules for the offset vectors, we start with the simplest case of a collision on a flat surface in the absence of an external field. As is easily seen, both the position components $\delta\mathbf{q} \equiv \{\delta x, \delta y\}$ and the momentum components $\delta\mathbf{p} \equiv \{\delta p_x, \delta p_y\}$ of the offset vector $\boldsymbol{\delta}$ are reflected on the surface. This means that their component normal to the surface changes its sign, whereas the component parallel to the surface remains unchanged.

Next we proceed to the case of the collision with a curved surface (Fig. 2) [24]. Here $\mathbf{p}$ is the momentum of the particle immediately before the collision and $\mathbf{p}'$ immediately after the collision. The vectors $\mathbf{t}$ and $\mathbf{t}'$ are unit vectors perpendicular to $\mathbf{p}$ and $\mathbf{p}'$, respectively. $\mathbf{h}$ is the principal normal vector given by $\mathbf{h}(s) = \ddot{\mathbf{k}}(s)/\kappa$, where $\mathbf{k}(s)$ is the surface of the scatterer parametrized by the arclength s and the double overdot indicates the second derivative with respect to s. Finally, $\kappa = |\ddot{\mathbf{k}}(s)|$ is the curvature of the obstacle, which is $1/R$ in our case.

It was demonstrated in a recent paper [24] that the transformation rule for $\delta\mathbf{q}$ is left unchanged by the curvature, but an additional term must be taken into account for the momentum-component transformation rule. Any offset $\delta\mathbf{q}$ in configuration space causes the collision point of the satellite trajectory to be displaced by the arclength δs from the collision point of the reference trajectory as

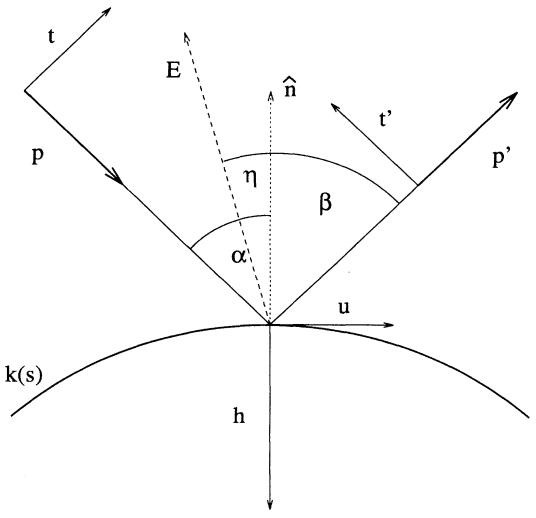

FIG. 2. The geometry of a collision. The symbols are explained in the main text.

shown in Fig. 3. This leads to a change in the angle of incidence of the satellite trajectory and consequently an additional term $\delta\mathbf{p}''$ in the corresponding transformation rule. Due to the displacement δs both the angle of incidence and the angle of reflection are altered by $\delta\phi = \kappa\delta s = \delta s/R$ and δs is given by $\delta s = \delta\mathbf{q}\cdot\mathbf{t}/\cos\alpha$. We finally obtain

$$\delta\mathbf{p} \to \delta\mathbf{p}' - 2\delta\phi p\mathbf{t}', \tag{16}$$

with

$$\delta\phi = \frac{\delta\mathbf{q}\cdot\mathbf{t}}{R\cos\alpha}. \tag{17}$$

The first term on the right-hand side of (16) is simply the reflection of $\delta\mathbf{p}$ whereas the second term is a consequence of the rotation of the outgoing momentum due to the curvature of the collision surface.

Finally, we have to take into account the action of the field and of the thermostat on the offset vectors during the collision. As before, the vector $\delta\mathbf{q}$ remains unaffected by the additional complication and is simply reflected. On the other hand, the transformation rule for $\delta\mathbf{p}$ must be adapted to the new situation. Since for the evaluation of the Lyapunov exponents only the linearized map relating $\{\delta\mathbf{q}, \delta\mathbf{p}\}$ immediately before and after the collision is needed, it suffices to treat the effects of the curved surface and of the field plus thermostat independently and then add the results. Hence, without loss of generality we consider a particle colliding with a flat surface under the influence of the original equations of motion (1) as shown in Fig. 4. The full line represents the reference trajectory whereas the broken line denotes the satellite trajectory separated by $\delta\mathbf{q}$ immediately before the collision. When the reference trajectory collides with the surface, the satellite trajectory is at a distance δu from its own collision point. We note that this distance can be positive

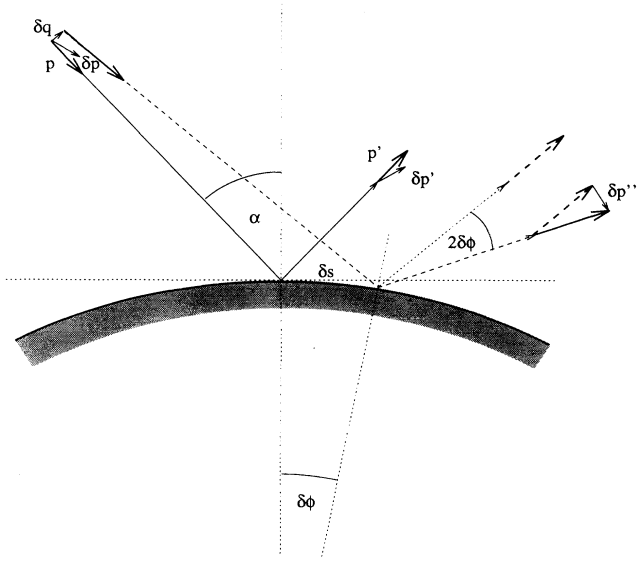

FIG. 3. The effect of a collision with a curved surface on the offset vectors in tangent space.

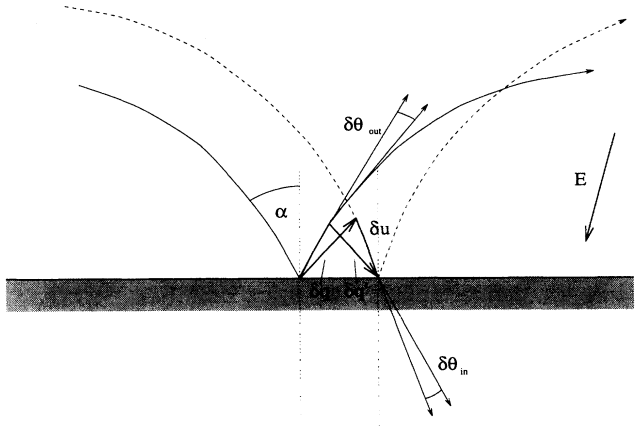

FIG. 4. The effect of a collision with a flat surface under the influence of an external field on the offset vectors in tangent space.

as well as negative. This provokes an infinitesimal temporal delay $\delta t = \delta u/(p/m)$ between the two collisions. During this short time interval the external field and the thermostat continue to reorient the momentum vectors both for the reference and for the offset trajectories, thus contributing another term for the transformation rules of the momentum components. To account for this effect we note from Fig. 4 that the distance δu, and hence the time interval $\delta t = \delta u/(p/m)$, may be expressed in terms of $\delta\mathbf{q}$ according to

$$\delta u = \delta\mathbf{q}\cdot\mathbf{t}\ \tan\alpha - \delta\mathbf{q}\cdot\mathbf{p}/p. \tag{18}$$

It follows from the equation of motion (4) for θ that during the time interval δt any momentum vector reorients by

$$\delta\theta = -\delta t\frac{E}{p}\sin(\theta - \phi). \tag{19}$$

This equation applies to both the reference and the offset trajectories. Since we have to take the rotation of both trajectories into account, the difference angle between the outgoing momenta immediately after the collision due to this effect is finally given by

$$\delta\theta = -\delta\mathbf{q}\cdot(\mathbf{t}\ \tan\alpha - \mathbf{p}/p) \times\frac{mE}{p^2}\{\sin(\theta_{\text{in}} - \phi) + \sin(\theta_{\text{out}} - \phi)\}, \tag{20}$$

where θ_{in} and θ_{out} are the respective orientations of the incoming and outgoing momenta of the reference trajectory.

Adding all our results together we obtain the exact linear transformation rules for the offset vectors $\boldsymbol{\delta} = \{\delta\mathbf{q}, \delta\mathbf{p}\}$ during a collision:

$$\begin{aligned}\delta\mathbf{q} &\to \delta\mathbf{q}',\\ \delta\mathbf{p} &\to \delta\mathbf{p}' - (2\delta\phi + \delta\theta)p\mathbf{t}',\end{aligned} \tag{21}$$

where $\delta\phi$ is given by Eq. (17) and $\delta\theta$ by Eq. (20). Thus we have collected all the ingredients needed for the calculation of the full Lyapunov spectrum for the driven and thermostatted Lorentz gas. The results of our numerical calculations are presented in the following section.

V. RESULTS

In all our numerical simulations we set the wanderer mass $m = 1$, the wanderer speed $v = p/m = 1$, and the radius of the scatterer $R = 1$. The unit of time is Rm/p and all Lyapunov exponents are given in units of p/Rm. We tabulate the field strength E in units of p^2/Rm and the conductivity κ in units of R/p. By identifying opposite sides of the elementary cell (Fig. 1), periodic boundary conditions are obtained. We choose the field to point into the direction of the positive y axis, which means that it is perpendicular to a row of nearest neighbors. The densities ρ for all our calculations are well above the limiting case of infinite horizon $\rho_\infty = \frac{3}{4}\rho_0$, where ρ_0 is the close-packed density. Between collisions with the scatterer the equations of motion of both the reference trajectory and the offset vectors were integrated by means of a fourth-order Runge-Kutta algorithm with a time step of $0.005Rm/p$ [35]. Whenever the wanderer happened to intersect the surface of the scatterer or the boundary of the simulation cell, the intersection point was determined numerically with an accuracy of about 10^{-5}. Depending on the nature of that point, either transformation rules or boundary conditions were applied to the trajectory and the offset vectors.

It turns out that the Lyapunov exponents converge rather quickly towards their limiting values. In Fig. 5 all nonvanishing Lyapunov exponents, normalized by their final value, are shown as a function of simulation time for the densities $\rho = 0.8\rho_0$ and $\rho = 0.99\rho_0$ and the field strengths $ERm/p^2 = 0.0$, 0.5, and 1.0. One can infer from this figure that the error for the Lyapunov exponents listed in the tables below does not exceed 0.2%.

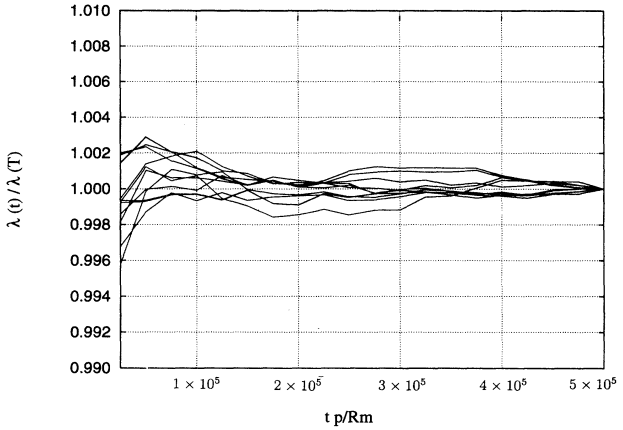

FIG. 5. The convergence of the maximum and minimum Lyapunov exponents for $\rho = 0.8\rho_0$ and $\rho = 0.99\rho_0$ and the field strengths $ERm/p^2 = 0.0$, 0.5, and 1.0 as a function of the reduced simulation time tp/Rm. The Lyapunov exponents are normalized by their final values. ρ_0 is the close-packed density.

Depending on the density, the number of collisions varied between 800 000 and 2×10^6 in all our simulations.

Our results are summarized in Tables I, II, and III for the respective three densities $\rho_1 = 0.8\rho_0$, $\rho_2 = 0.88\rho_0$, and $\rho_3 = 0.99\rho_0$. For each density we varied the field from $ERm/p^2 = 0$ to 2.5 in steps of 0.125. Figure 6 shows the maximum and minimum Lyapunov exponents for the three densities mentioned above as a function of the field strength. For each density the absolute value of the exponents decreases with increasing E, which means

TABLE I. Summary of results for a density $\rho = 0.8\rho_0$. r is the collision rate of the particle with the scatterer. The conductivity κ is given in units of R/p and the Lyapunov exponents in units of p/Rm.

EmR/p^2	r	κ	$\lambda_{\max}$	$\lambda_{\max}^{\mathrm{WCA}}$	$\lambda_{\min}$	$\lambda_{\min}^{\mathrm{WCA}}$	D_{KY}	D_1	ΔD_{KY}	ΔD_1
0.000	1.682		1.961	1.967	-1.961	-1.966	4.000	3.96	0.0000	0.04
0.125	1.682	0.191	1.958		-1.961		3.998		0.0015	
0.250	1.688	0.169	1.947		-1.958		3.994		0.0054	
0.375	1.694	0.175	1.931		-1.955		3.987		0.0126	
0.500	1.699	0.185	1.900	1.889	-1.946	-1.948	3.976	3.94	0.0238	0.06
0.625	1.698	0.187	1.862		-1.935		3.962		0.0378	
0.750	1.703	0.177	1.817		-1.917		3.947		0.0522	
0.875	1.716	0.161	1.775		-1.898		3.934		0.0652	
1.000	1.726	0.154	1.724	1.721	-1.879	-1.889	3.917	3.88	0.0821	0.12
1.125	1.754	0.147	1.680		-1.867		3.899		0.1001	
1.250	1.774	0.143	1.632		-1.856		3.879		0.1206	
1.375	1.779	0.149	1.563		-1.846		3.846		0.1531	
1.500	1.779	0.146	1.500	1.482	-1.829	-1.835	3.820	3.79	0.1800	0.21
1.625	1.769	0.146	1.425		-1.812		3.786		0.2134	
1.750	1.764	0.150	1.343		-1.804		3.744		0.2556	
1.875	1.723	0.145	1.266		-1.779		3.712		0.2880	
2.000	1.698	0.130	1.229	1.278	-1.752	-1.825	3.701	3.69	0.2981	0.31
2.125	1.650	0.125	1.204		-1.772		3.679		0.3203	
2.250	1.597	0.117	1.196		-1.791		3.667		0.3322	
2.375	1.599	0.110	1.160		-1.783		3.650		0.3493	
2.500	1.582	0.114	1.052	1.055	-1.769	-1.791	3.595	3.60	0.4049	0.40

TABLE II. Summary of results for a density $\rho = 0.8821\rho_0$. r is the collision rate of the particle with the scatterer. The conductivity κ is given in units of R/p and the Lyapunov exponents in units of p/Rm.

EmR/p^2	r	κ	$\lambda_{\max}$	$\lambda_{\max}^{\mathrm{WCA}}$	$\lambda_{\min}$	$\lambda_{\min}^{\mathrm{WCA}}$	D_{KY}	D_1	ΔD_{KY}	ΔD_1
0.000	2.544		2.466	2.456	-2.466	-2.455	4.000	3.96	0.0000	0.04
0.125	2.546	0.116	2.463		-2.465		3.999		0.0007	
0.250	2.545	0.113	2.451		-2.458		3.997		0.0029	
0.375	2.547	0.117	2.434		-2.451		3.993		0.0067	
0.500	2.553	0.113	2.411	2.401	-2.439	-2.432	3.988	3.96	0.0116	0.04
0.625	2.554	0.118	2.377		-2.423		3.980		0.0192	
0.750	2.550	0.118	2.336		-2.403		3.972		0.0278	
0.875	2.551	0.116	2.287		-2.377		3.962		0.0376	
1.000	2.570	0.106	2.238	2.233	-2.344	-2.348	3.954	3.92	0.0454	0.08
1.125	2.595	0.101	2.182		-2.311		3.944		0.0557	
1.250	2.616	0.096	2.131		-2.281		3.934		0.0659	
1.375	2.636	0.094	2.068		-2.247		3.920		0.0795	
1.500	2.656	0.096	2.009	1.998	-2.227	-2.240	3.902	3.88	0.0978	0.12
1.625	2.680	0.100	1.949		-2.214		3.880		0.1198	
1.750	2.670	0.102	1.886		-2.200		3.857		0.1424	
1.875	2.660	0.103	1.837		-2.200		3.835		0.1649	
2.000	2.650	0.102	1.822	1.816	-2.233	-2.270	3.816	3.81	0.1839	0.19
2.125	2.614	0.103	1.785		-2.252		3.792		0.2072	
2.250	2.573	0.100	1.726		-2.232		3.773		0.2267	
2.375	2.547	0.096	1.675		-2.220		3.754		0.2456	
2.500	2.542	0.093	1.618	1.586	-2.199	-2.208	3.735	3.72	0.2643	0.28

that the field tends to make the trajectory of the particle less chaotic. In fact, in the presence of a strong field the momentum vector of the particle quickly turns into the field direction after each collision, whereas in the equilibrium case two decorrelated trajectories always remain decorrelated. With a fixed field strength the maximum exponent increases with density due to an increase of the collision rate.

We have already mentioned that for dissipative systems the phase space density collapses onto a strange attractor with an information dimension D_1 smaller than the dimension of the embedding phase space. As shown in Fig. 7, this dimensional reduction $\Delta D_{\mathrm{KY}} = 4 - D_{\mathrm{KY}}$, calculated with the Kaplan-Yorke conjecture (12) from the Lyapunov spectrum, grows with increasing field strength. This effect is small for high densities, but be-

TABLE III. Summary of results for a density $\rho = 0.9924\rho_0$. r is the collision rate of the particle with the scatterer. The conductivity κ is given in units of R/p and the Lyapunov exponents in units of p/Rm.

EmR/p^2	r	κ	$\lambda_{\max}$	$\lambda_{\max}^{\mathrm{WCA}}$	$\lambda_{\min}$	$\lambda_{\min}^{\mathrm{WCA}}$	D_{KY}	D_1	ΔD_{KY}	ΔD_1
0.000	5.725		3.589	3.423	-3.589	-3.420	4.000	3.96	0.0000	0.04
0.125	5.731	0.011	3.586		-3.586		4.000		0.0000	
0.250	5.731	0.012	3.578		-3.578		3.999		0.0002	
0.375	5.742	0.012	3.567		-3.568		3.999		0.0005	
0.500	5.753	0.012	3.552	3.395	-3.555	-3.404	3.999	3.96	0.0009	0.04
0.625	5.761	0.013	3.530		-3.535		3.998		0.0014	
0.750	5.781	0.012	3.504		-3.512		3.997		0.0021	
0.875	5.800	0.013	3.473		-3.483		3.997		0.0029	
1.000	5.813	0.013	3.432	3.280	-3.445	-3.318	3.996	3.96	0.0038	0.04
1.125	5.844	0.012	3.384		-3.400		3.995		0.0046	
1.250	5.859	0.011	3.328		-3.346		3.994		0.0055	
1.375	5.896	0.010	3.269		-3.289		3.993		0.0062	
1.500	5.889	0.009	3.197	3.085	-3.218	-3.162	3.993	3.96	0.0067	0.04
1.625	5.883	0.008	3.122		-3.146		3.992		0.0075	
1.750	5.864	0.008	3.042		-3.067		3.991		0.0083	
1.875	5.868	0.008	2.961		-2.990		3.990		0.0096	
2.000	5.869	0.007	2.878	2.805	-2.909	-2.918	3.989	3.95	0.0106	0.05
2.125	5.906	0.007	2.789		-2.824		3.987		0.0121	
2.250	5.929	0.007	2.695		-2.733		3.986		0.0139	
2.375	5.929	0.008	2.599		-2.644		3.983		0.0170	
2.500	5.906	0.006	2.498	2.466	-2.539	-2.591	3.984	3.94	0.0160	0.06

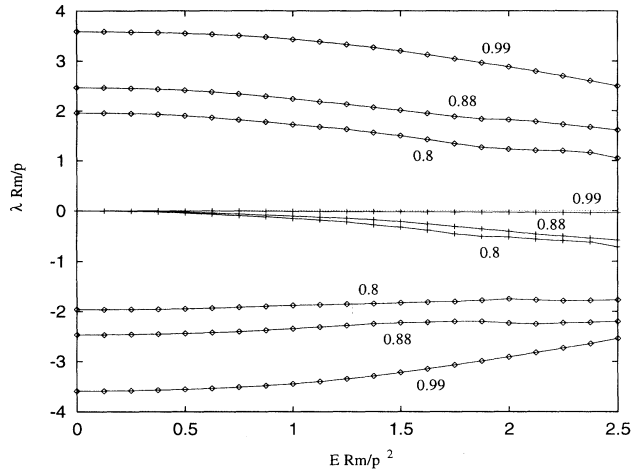

FIG. 6. Maximum and minimum Lyapunov exponent for the densities $\rho = 0.8\rho_0$, $\rho = 0.88\rho_0$, and $\rho = 0.99\rho_0$ as a function of the reduced field strength ERm/p^2. The crosses denote the sum $\lambda_{\max} + \lambda_{\min}$. All exponents are plotted in reduced units.

comes very pronounced for low densities.

A two-dimensional Poincaré map is obtained if the points $(\eta, \sin\beta)$ for successive collisions of the wanderer with the scatterer are displayed. According to Fig. 2, η is the angle between the normal vector $\hat{\mathbf{n}}$ at the collision point and the field direction and $\beta = \theta - \eta$ is the angle between the outgoing momentum and $\hat{\mathbf{n}}$. An example is shown in Fig. 8 for a density $\rho = 0.88\rho_0$ and a field strength $ERm/p^2 = 2.5$. All points in the chaotic sea belong to a single trajectory. The two seemingly closed lines point to the existence of regular trajectories located in a regular subspace of the phase space [5]. The multifractal properties of the chaotic trajectory have been analyzed by determining the singularity spectrum $f(a)$ [34]. The values for the information dimension D_1 deduced from $f(a)$ are also included in the Tables I–III. The difference between these numbers and the much more accurate values for D_{KY} are solely due to the lower numerical accuracy of the box-counting algorithm employed for the computation of $f(a)$.

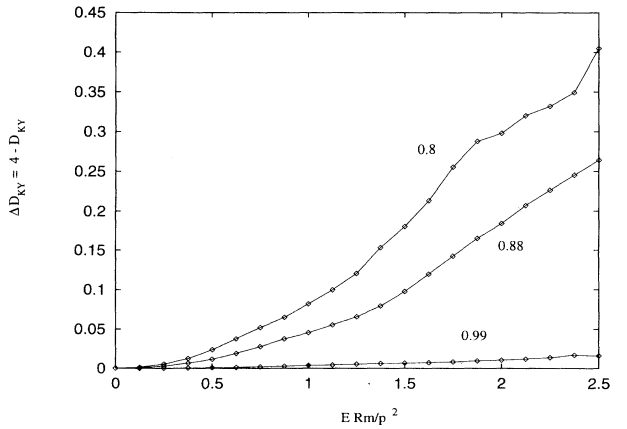

FIG. 7. Dimensionality reduction $\Delta D_{\mathrm{KY}} = 4 - D_{\mathrm{KY}}$ as a function of the reduced field strength ERm/p^2 for the densities $\rho = 0.8\rho_0$, $\rho = 0.88\rho_0$, and $\rho = 0.99\rho_0$.

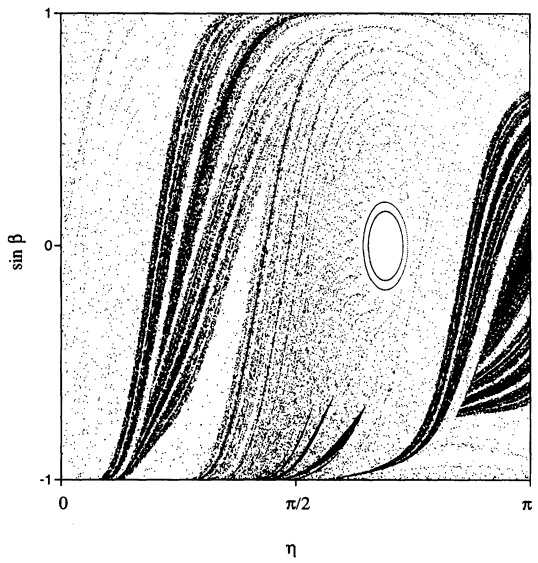

FIG. 8. Poincaré plot for the collision parameters η and $\sin\beta$ at a density of $\rho = 0.88\rho_0$ and a field strength $ERm/p^2 = 2.5$. According to Fig. 2 η is the angle between the normal vector $\hat{\mathbf{n}}$ at the collision point and the field direction, and $\beta = \theta - \eta$ is the angle between the outgoing momentum immediately after the collision and the normal vector $\hat{\mathbf{n}}$.

Figure 9 shows the dependence of the nonlinear conductivity as a function of E. With the exception of small fluctuations, κ is an overall decreasing function of the field strength, which is a consequence of the external field combined with the thermostat. For strong fields

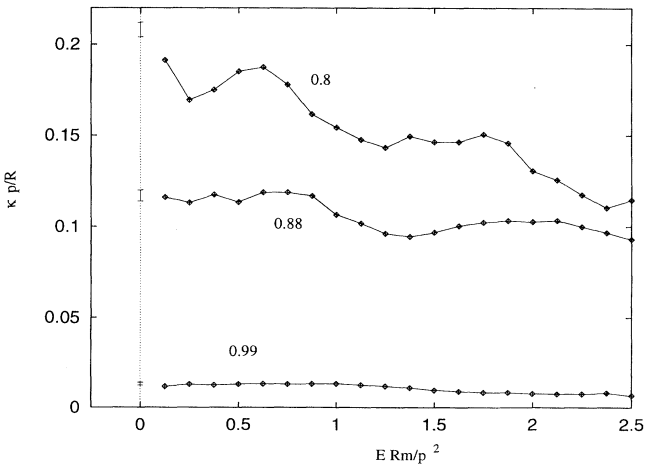

FIG. 9. Nonlinear conductivity κ as a function of the field strength E for three different densities $\rho/\rho_0 = 0.8, 0.88$, and 0.99. The error bars for $E = 0$ denote the linear response value of κ obtained with the Green-Kubo relation from the velocity autocorrelation function. All quantities are given in reduced units.

the momentum of the particle reorients into the field direction within a short time after each collision. Thus the particle spends most of its time traveling with constant speed in the approximate field direction and cannot be accelerated further by stronger fields. Only collisions can offset the action of the field. It follows that the conductivity decreases with increasing density. For the limiting case of very weak fields the nonlinear conductivity converges towards the linear response value calculated from the Green-Kubo relation in the absence of an external field. These linear response results are denoted by the error bars in Fig. 9 (for $E = 0$). All conductivities obtained in this work agree also well with the results of Moran and Hoover [5].

The conductivity κ can be calculated also directly from the Lyapunov spectrum according to Eq. (10). Within the resolution of Fig. 9 these numbers are indistinguishable from those obtained from the time-averaged current.

In the past Lyapunov spectra of systems with elastic hard interactions have also been estimated by replacing the singular potential with a very steep but nevertheless smooth potential [7]. To test this procedure we perform a series of simulations with a system, where the wanderer and the scatterer interact according to [7]

$$V(r) = \begin{cases} \infty \quad \text{for } r \le R \\ 4\epsilon \left[\left(\frac{\sigma}{R-r} \right)^{12} - \left(\frac{\sigma}{R-r} \right)^{6} \right] + \epsilon \\ \text{for } \; R < r \le R + 2^{1/6}\sigma \\ 0 \quad \text{for } \; R + 2^{1/6}\sigma < r, \end{cases} \tag{22}$$

a generalization of the Weeks-Chandler-Anderson potential. The parameter σ determines the thickness of the interaction layer surrounding the scatterer. In this paper we use $\sigma = 0.1R$ and $\epsilon = 0.5p^2/m$. Since the potential is very steep, a Runge-Kutta algorithm with adaptive step size was used for the integration of the equations of motion. The Lyapunov spectrum was determined with the classic algorithm of Benettin *et al.*. The results of these simulations are also included in Tables I–III and are denoted by $\lambda_{\max}^{\mathrm{WCA}}$ and $\lambda_{\min}^{\mathrm{WCA}}$. For low densities the results of both methods agree within $0.2-1.5\,\%$, whereas at high densities they display discrepancies of the order $2-5\,\%$. This may be attributed to the overlap of the thin interaction layer at high densities.

VI. CONCLUSION

In this work an algorithm for the evaluation of the full Lyapunov spectrum for the nonequilibrium Lorentz gas is presented. It generalizes the classic method of Benettin *et al.* to include elastic hard-core collisions in the presence of an external field and of a Gaussian thermostat. Both the intercollisional and collisional contributions are treated exactly. The algorithm does not require the construction of Poincaré plots and may be easily generalized to the treatment of (a) random arrangement of scatterers, (b) other types of hard systems in nonequilibrium states such as the Lorentz gas with shearing boundary conditions, and (c) hard many-body systems in two or three dimensions, subjected to arbitrary external perturbations. The method is also well suited to accurately quantifying the shifts of conjugate pairs of Lyapunov exponents in nonequilibrium steady state systems [25] and to determine the corrections expected for a finite number of particles [36,25].

ACKNOWLEDGMENTS

We gratefully acknowledge the financial support from the Fonds zur Förderung der Wissenschaftlichen Forschung, Grant No. P09677, and the generous allocation of computer resources by the Computer Center of the University of Vienna. We thank J. R. Dorfman, W. G. Hoover, and M. Vencour for their interest in this work and for stimulating discussions and G. P. Morriss for sending us a copy of Ref. [23] prior to publication.

[1] J. Machta and R. Zwanzig, Phys. Rev. Lett. **50**, 1959 (1983).
[2] W. G. Hoover, J. Stat. Phys. **42**, 587 (1986).
[3] W. G. Hoover, B. Moran, C. G. Hoover, and W. J. Evans, Phys. Lett. A **133**, 114 (1988).
[4] H. van Beijeren and J. R. Dorfman, Phys. Rev. Lett. **74**, 4412 (1995).
[5] B. Moran and W. G. Hoover, J. Stat. Phys. **48**, 709 (1987).
[6] N. J. Chernov, G. L. Eyink, J. L. Lebovitz, and Ya. G. Sinai, Commun. Math. Phys. **154**, 569 (1993).
[7] A. Baranyai, D. J. Evans, and E. G. D. Cohen, J. Stat. Phys. **70**, 1085 (1993).
[8] W. G. Hoover, C. G. Hoover, W. J. Evans, B. Moran, J. A. Levatin, and E. A. Craig, in *Microscopic Simulations of Complex Flows*, Vol. 236 of *NATO Advanced Study Institute, Series B: Physics*, edited by M. Mareshal (Plenum, New York, 1990), p. 199.
[9] G. P. Morriss, Phys. Rev. A **39**, 4811 (1989).
[10] J. Petravic, D. J. Isbister, and G. P. Morriss, J. Stat. Phys. **76**, 1045 (1994).
[11] D. J. Evans and G. P. Morriss, *Statistical Mechanics of Nonequilibrium Liquids* (Academic, London, 1990).
[12] W. G. Hoover, *Computational Statistical Mechanics* (Elsevier, Amsterdam, 1991).
[13] W. N. Vance, Phys. Rev. Lett. **69**, 1356 (1992).
[14] W. G. Hoover and B. Moran, Phys. Rev. A **40**, 5319 (1989).
[15] L. A. Bunimovich and Ya. G. Sinai, Commun. Math. Phys. **73**, 247 (1980).
[16] L. A. Bunimovich and Ya. G. Sinai, Commun. Math. Phys. **78**, 471 (1981).
[17] P. Gaspard and G. Nicolis, Phys. Rev. Lett. **65**, 1693 (1990).
[18] P. Gaspard and F. Baras, in *Microscopic Simulations of Complex Hydrodynamic Phenomena*, Vol. 292 of *NATO*

Advanced Study Institute, Series B: Physics, edited by M. Mareshal and B. Holian (Plenum, New York, 1992), p. 301.
[19] G. Benettin, L. Galgani, A. Giorgilli, and J.-M. Strelcyn, Meccanica **15**, 9 (1980).
[20] A. Wolf, J. B. Swift, H. L. Swinney, and J. A. Vastano, Physica D **16**, 285 (1985).
[21] P. Cvitanović, P. Gaspard, and T. Schreiber, Chaos **2**, 85 (1992).
[22] G. P. Morriss and L. Rondoni, J. Stat. Phys. **76**, 553 (1994).
[23] J. Lloyd, M. Niemeyer, L. Rondoni, and G. P. Morriss, Chaos (to be published).
[24] Ch. Dellago and H. A. Posch, Phys. Rev. E **52**, 2401 (1995).
[25] Ch. Dellago, H. A. Posch, and W. G. Hoover (unpublished).
[26] V. I. Oseledec, Trans. Moscow Math. Soc. **19**, 197 (1968).
[27] H. A. Posch and W. G. Hoover, Phys. Rev. A **38**, 473 (1988).
[28] H. A. Posch and W. G. Hoover, Phys. Rev. A **39**, 2175 (1989).
[29] D. J. Evans, E. G. D. Cohen, and G. P. Morriss, Phys. Rev. A **42**, 5990 (1990).
[30] H. A. Posch and W. G. Hoover, in *Molecular Liquids, New Perspectives in Physics and Chemistry*, Vol. 379 of *NATO Advanced Study Institute, Series C: Mathematical and Physical Sciences*, edited by José J. C. Teixeira-Dias (Kluwer, Dordrecht, 1992), p. 527.
[31] P. Grassberger, Phys. Lett. **97A**, 227 (1983).
[32] H. G. E. Hentschel and I. Procaccia, Physica D **8**, 435 (1983).
[33] M. H. Jensen, L. P. Kadanoff, and I. Procaccia, Phys. Rev. A **36**, 1409 (1987).
[34] A. Chabra and R. V. Jensen, Phys. Rev. Lett. **62**, 1327 (1989).
[35] F. J. Vesely, *Computational Physics, An Introduction* (Plenum, New York, 1994).
[36] E. G. D. Cohen, Physica A **213**, 293 (1995).

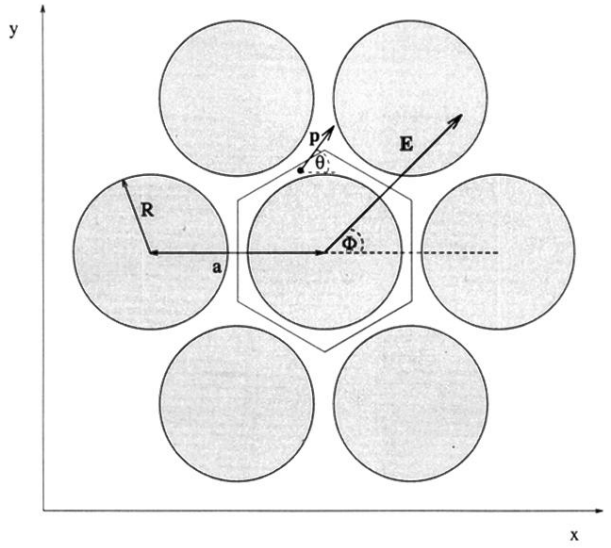

FIG. 1. The geometry of the periodic Lorentz gas.